applied sciences

MDPI

Article

Are Suprapectineal Quadrilateral Surface Buttressing Plates Performances Superior to Traditional Fixation? A Finite Element Analysis

Mara Terzini [1,2], Andrea Di Pietro [1], Alessandro Aprato [3], Stefano Artiaco [3], Alessandro Massè [3] and Cristina Bignardi [1,2,*]

[1] Department of Mechanical and Aerospace Engineering (DIMEAS), Politecnico di Torino, 10129 Turin, Italy; mara.terzini@polito.it (M.T.); andrea.dipietro94@gmail.com (A.D.P.)
[2] Polito[BIO]Med Lab, Politecnico di Torino, 10129 Turin, Italy
[3] School of Medicine, University of Turin, Via Zuretti 29, 10133 Turin, Italy; ale_aprato@hotmail.com (A.A.); sartiaco@cittadellasalute.to.it (S.A.); alessandro.masse@unito.it (A.M.)
* Correspondence: cristina.bignardi@polito.it

Featured Application: The article illustrates the biomechanical analysis of a new suprapectineal plate; the personalized bended geometry of the plate was derived from the undeformed commercial device and its performance data were reported and can be used as a reference.

Abstract: Acetabular fractures have a high impact on patient's quality of life, and because acetabular fractures are high energy injuries, they often co-occur with other pathologies such as damage to cartilage that could increase related morbidity; thus, it appears of primary importance developing reliable treatments for this disease. This work aims at the evaluation of the biomechanical performances of non-conservative treatments of acetabular fractures through a finite element approach. Two pelvic plates models (the standard suprapectineal plate—SPP, and a suprapectineal quadrilateral surface buttressing plate—SQBP) were analyzed when implanted on transverse or T-shaped fractures. The plates geometries were adapted to the specific hemipelvis, mimicking the bending action that the surgeon performs on the plate intraoperatively. Implemented models were tested in a single leg stance condition. The obtained results show that using the SQBP plate in transverse and T-shaped acetabular fractures generates lower bone stress if compared to the SPP plate. Interfragmentary movement analysis shows that the SQBP plate guarantees greater stability in transverse fractures. In conclusion, the SQBP plate seems worthy of further clinical analysis, having resulted as a promising option in the treatment of transverse and T-shaped acetabular fractures, able to reduce bone stress values and to get performances comparable, and in some cases superior, to traditional fixation.

Keywords: fracture synthesis; internal fixation; stress analysis; interfragmentary movement analysis; suprapectineal plates

Citation: Terzini, M.; Pietro, A.D.; Aprato, A.; Artiaco, S.; Massè, A.; Bignardi, C. Are Suprapectineal Quadrilateral Surface Buttressing Plates Performances Superior to Traditional Fixation? A Finite Element Analysis. *Appl. Sci.* **2021**, *11*, 858. https://doi.org/10.3390/app11020858

Received: 14 December 2020
Accepted: 15 January 2021
Published: 18 January 2021

1. Introduction

Acetabular fractures are relatively uncommon, with an incidence rate ranging from 3 to 8.1 cases/100,000 person/year. These fractures have a high impact on patient quality life and are mostly seen in younger patients and persons aged over 50 years old [1,2]. Traditionally, acetabular fractures are classified according to Letournel classification into ten major fracture patterns, which consist of five simple patterns and five complex patterns [3,4]. Due to the complexity of the pelvic anatomic structure, acetabular fractures represent a challenging procedure for orthopedic surgeons.

At present, a well-established surgical procedure in the treatment of acetabular fractures is represented by the anterior intrapelvic approach (AIP) [5–7]; this technique allows for the minimization of operation times and risks related to blood loss during surgical

intervention [5,6]. At any rate, the purpose of the surgical treatment is the achievement of anatomical reduction and stable fixation. In transverse and T-shaped fractures there is no bony structure able to oppose to medial subluxation of the femoral head since the entire medial wall is detached from the superior aspect of the dome. Therefore, systems able to fix both columns are traditionally used in these fracture patterns. Recently, a new pre-contoured anatomic plate design has been developed aiming at fixation of both column and quadrilateral plate [8]. Its anatomic shape was designed to be implanted with its native curvature, but this latter could not be always adequate to perfectly match to the bone shape. Thus, further in-situ bending is often indispensable [6], with a consequent increase in surgical times and modification of the performance of the native device.

In this framework, a lack of biomechanical data regarding these plates in operative conditions emerges. Many examples are present in the literature about transforming the qualitative assessment of clinical problems to quantitative by exploiting numerical modeling [9–15]. Here, finite element modeling was used to biomechanically examine different bone-plates configurations.

The aim of this study is therefore to compare the stability guaranteed by two different suprapectineal plates: (1) a standard pelvic plate (SPP) and (2) a suprapectineal quadrilateral surface buttressing plate (SQBP).

2. Materials and Methods

2.1. The Bone-Plate Configurations

2.1.1. Patient-Adapted Plate Geometry Generation

The starting point of the geometry generation was a physical SQBP plate (Pro suprapectineal Stryker plate—Stryker, Kalamazoo, MI, US), from which both the SQBP and SPP geometries were obtained. The two plates, indeed, share the same suprapectineal portion, intended for placement on the arcuate line of the pelvic brim, but the former has an additional portion lying on the infrapectineal side of the pelvis, intended to fit the quadrilateral surface of the ilium.

Following the principles of reverse engineering and studying the SQBP plate characteristic shapes, the following steps have been followed to reproduce every feature of the undeformed plate in the CAD environment (Rhinoceros 3D, Associates, Seattle, WA, USA):

- The whole plate profile was drawn lying on a plane, and extruded (thickness equal to 2 mm) thus obtaining a solid (Figure 1a).
- The suprapectineal portion of the plate was bent in order to recreate an anatomic curvature which follows the arcuate line of the ilium. The bending has been performed in the x-y plane along the z axis so that, at the end of this step, the plate still lies on the x-y plane (Figure 1b)
- The infrapectineal portion of the plate was bent with a 90° curvature with respect to the x-y plane and, afterward, was inflected along the z axis to fit to the quadrilateral surface of the ilium (Figure 1c).

The so obtained undeformed plate geometry was then morphed on the hemipelvis CAD geometry (a standard Sawbones right hemipelvis—SKU: 3415-1—Sawbones®, Europe AB, Malmoe, Sweden) in the Hyperworks environment (Altair Engineering, Inc., Troy MI, United States) to obtain a patient-adapted geometry. In detail, the suprapectineal side of the already meshed plate (see Section 2.2.1) was adapted to the bone surface exploiting the *freehand* command of Hypermorph. Through the *freehand* command some nodes of the plate were projected on the surface using the *move node to surface* option and setting command parameters exploiting a trial and error procedure. After morphing, the plate hole countersinks were obtained by Boolean differences between the plate and spheres of 3.5 mm radius after having mathematically defined their center locations.

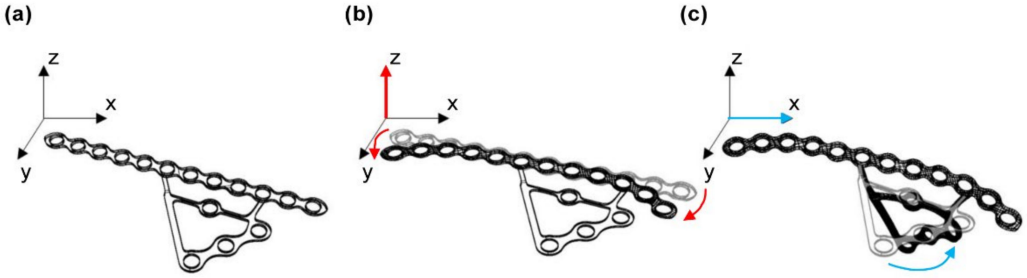

Figure 1. Patient-adapted plate geometry generation through extrusion (**a**), on-plane bending along the z-axis, shown in red (**b**) and off-plane bending along the x-axis, shown in blue (**c**).

Starting from the patient-adapted SQBP plate design, the SPP geometry was derived by deleting the infrapectineal portion of the plate. The two obtained geometries are shown in Figure 2.

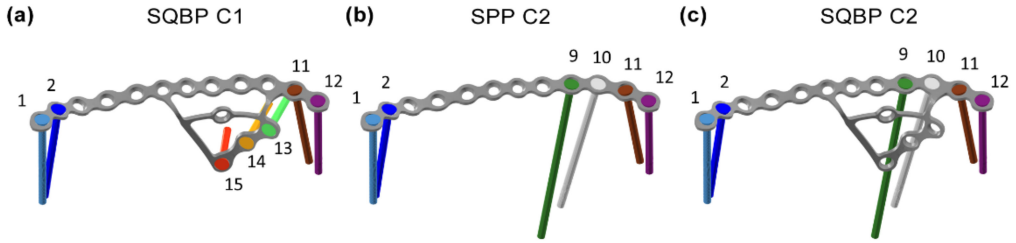

Figure 2. Generated plates geometry assembled with the screws configuration to obtain the three plate-screws models: (**a**) suprapectineal quadrilateral surface buttressing plate (SQBP) C1, (**b**) SPP C2 and (**c**) SQBP C2.

2.1.2. The Plate-Screws Models

Combining plate typologies (SPP and SQBP) and screws configurations (C1 and C2, as will be explained in the following), three plate-screws models were implemented, one of which represents a mixed configuration composed of the SQBP plate without the screws inserted into the quadrilateral surface of the ilium. This latter configuration was implemented in order to evaluate the stabilization contribution of the infrapectineal side of the plate when not anchored to the bone (Figure 2c). Indeed, the presence of the infrapectineal portion of the SQBP plate in simple contact with the quadrilateral surface of the ilium could, alone, hinder the sliding motions in the fracture plane thus ensuring improved stability compared to the standard SPP plate.

Accordingly, two different screw fixation configurations have been developed: the configuration C1 is composed of seven screws, four screws placed at the two extremity of the plate on the iliopectineal brim (1, 2, 11, 12 in Figure 2a), and the other three (13, 14, 15 in Figure 2a) inserted on the quadrilateral surface of the ilium, taking care not to penetrate the acetabulum; the configuration C2 is composed of six screws, each one belonging to the arcuate line of ilium; two long screws in the middle portion of the plate (9, 10 in Figure 2b) are longer than the others, reaching 89 mm in length, in order to cross the fracture line, thus holding onto the detached bone component. Screws length for each configuration were defined according to clinicians' indications, and consistently with the hemipelvis geometry. This is, indeed, common practice during surgery, being screw length selected to be suitably positioned without protruding from the second cortex.

The screws simplified geometry was obtained in Rhinoceros through the union of solids: a hemisphere (radius 1.75 mm) as screw head and a cylinder (radius 1.25 mm) as screw body. The presence of threads was neglected in order to reduce the computational costs. Figure 2 shows the three plate-screws models considered in this study, while Table 1 lists the screws length.

Table 1. Length of the screws (in mm) selected for the C1 and C2 configurations.

Screw N°	Configuration C1 [1]	Configuration C2 [1]	Length (mm)
1	X	X	48
2	X	X	48
9		X	89
10		X	79
11	X	X	40
12	X	X	43
13	X		29
14	X		29
15	X		22

[1] Symbol X identifies screw considered in the specific configuration.

2.1.3. The Acetabular Fractures

The femoral loads are in direct contact with the acetabular fracture, and a simplification of the boundary conditions in this region would influence the distribution of the results. For this reason, in the acetabular region, a cartilage volume having a thickness of 2 mm was created to improve stress distribution reliability [16]. Moreover, a femoral component simulacrum with a femoral head of 17.5 mm of radius was created for load application (see Section 2.2.4). Two typologies of acetabular fractures have been then considered, being the most frequent ones [17]: the elementary transverse and the so called T-shaped one. The fractures were generated after meshing (see Section 2.2.1) by manually deleting elements: the obtained fracture gap thickness varies from 2 to 3 mm.

From the combination of fracture types and plate-screw models, a total of six bone-plate configurations were obtained, as visible in Figure 3.

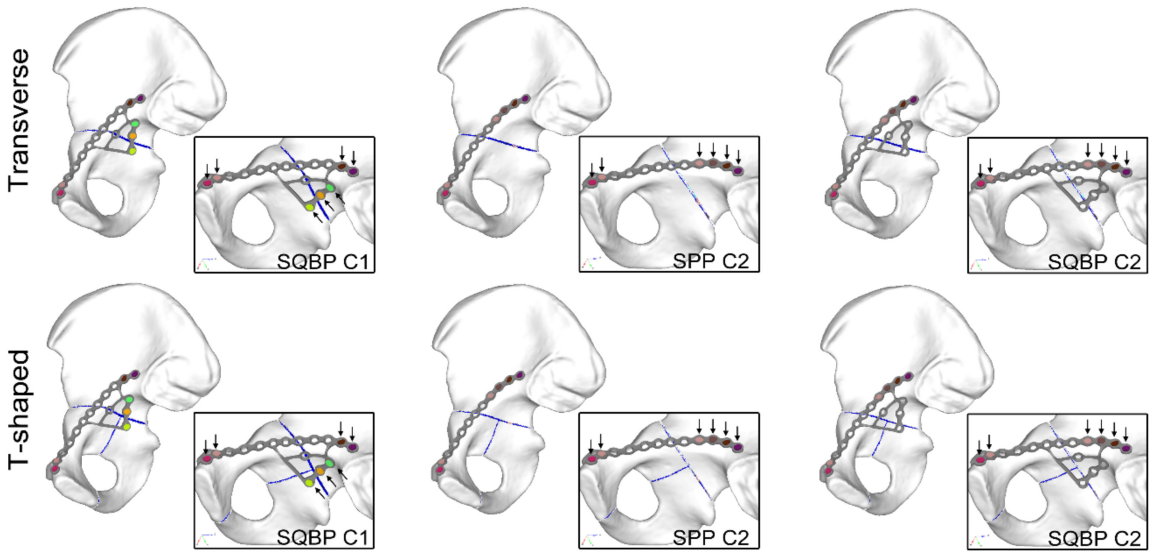

Figure 3. Six implemented models arranged according to plate-screw configuration (on the rows) and fracture typology (on the column). The femoral component simulacrum was here hidden for sake of clarity. The figures inside the black boxes provide a view of the plated region, allowing to focus on the screws configurations (black arrows) and on the implemented fractures.

2.2. Finite Element Models

2.2.1. Meshing

Meshing was performed in the Hypermesh environment adopting, where possible, mesh sharing techniques, aiming at reducing computational costs. A congruent mesh was therefore created between: (1) cortical and cancellous bone, (2) cartilage and bone

and (3) screws and bone, at the portion of the screws located in contact with bone. The screw-bone interfaces were therefore modeled as fully bonded [18,19], assuming a complete osseous integration between screws and living tissues, which results in the continuity of the displacement field at the interface.

The volumetric mesh of the SQBP plate and the SPP plate were created in order to maintain the same discretization in their suprapectineal common portion. According to components minimum dimensions, elements global edge lengths ranges between 0.56 and 1.65 mm (Table 2). Figure 4 shows the mesh generated for a representative model.

Table 2. Number of elements, elements global edge length and element type for each models' component.

Component	Number of Elements	Global Edge Length (mm)	Element Type
Transverse fractured Bone	1,774,743	1.50	Tetra4
T-shaped fractured Bone	1,772,012	1.45	Tetra4
Configuration screw C1	22,043	0.89	Tetra4
Configuration screw C2	27,666	0.73	Tetra4
SQBP plate	49,715	0.66	Tetra4
SPP plate	37,070	0.56	Tetra4
Cartilage in transverse fracture	24,915	0.65	Penta6
Cartilage in T-shaped fracture	24,520	0.70	Penta6
Femur simulacrum	169,818	1.65	Tetra4

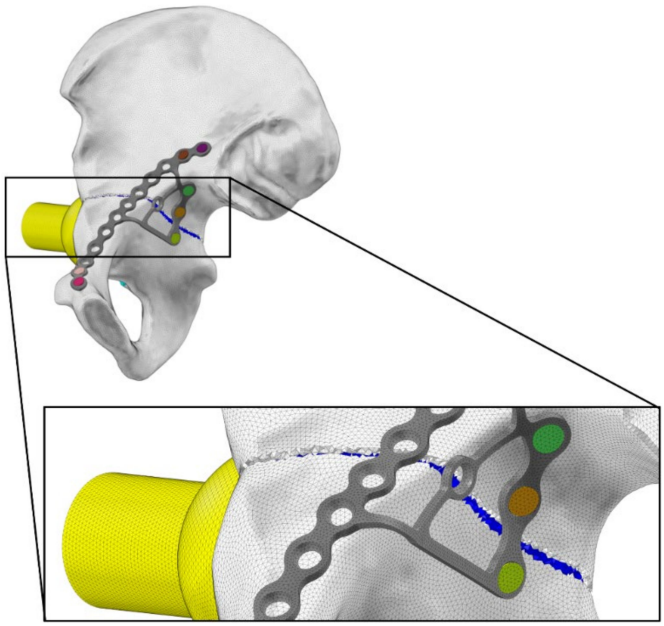

Figure 4. Mesh generated with a zoomed detail of the fractured region. The SQBP C1 plate-screw model implanted on a transverse fracture is shown as a representative.

The mean simulation time for each model is equal to 40 min adopting an intel® Core™ i7 8th gen CPU @3.6 GHz with 13 GB RAM dedicated.

2.2.2. Mechanical Properties

Elastic materials with isotropic properties were assigned to bony and metallic components (Table 3). The cartilage was modeled as a non-linear hyperelastic material of the neo-Hookean type [20] (E = 12 MPa and ν = 0.46 [21]).

Table 3. Components material properties.

Material	Elastic Modulus E (MPa)	Poisson's Ratio ν	Density δ (Kg/m^3)
Cortical bone [22]	16,700	0.300	1600
Cancellous bone [22]	1000	0.055	640
Screws and plate [23]	193,000	0.290	8000

2.2.3. Contact Implementation

As previously mentioned, the contact implementation was avoided where possible by adopting a congruent mesh, de facto a substitute for a tied contact. Nevertheless, frictional contacts (Table 4) were defined between: (1) the femur simulacrum and the cartilage to allow for the loading transfer; (2) the screws head and the plate and between plate and bone to implement screws preload; (3) bone and bone, to detect self-contacts in the fracture region.

Table 4. Static friction coefficients considered for each components pair.

Components Pair	Static Friction Coeff.
Femur simulacre—Cartilage	0.02 [24,25]
Plate—Bone	0.37 [24]
Plate—Screw	0.10 [26]
Bone—Bone	0.40 [24]

2.2.4. Boundary Conditions

Plates performances were assessed during a single-leg stance simulation. To reproduce plates implant, a preliminary screws pre-loading step was implemented, accounting for the screws fastening performed by the surgeon. The screws pre-loading was performed exploiting bolt elements and imposing a 50 N load collinear to the screw axis, resulting from the torque generated by the surgeon during surgery. It is well known that only a small percentage of the applied torque produces the effective pre-tensioning of the screw, while the major amount is lost to overcome the friction between threads and bone. Indeed, in the most unfavorable condition only 5% of the applied torque is useful for pre-tensioning [27]. In this work, 10% of the applied torque (4 Nm [28–30]) was considered for the screws pre-load, and the conversion from torque to axial load was done according to Karnezis and colleagues [31] and rescaling their results to a 2.5 mm screw. It should be noted that no prestress perpendicular to the screw axis induced in the bone due to insertion of the threaded screw was considered. Despite this approach could influence the accuracy of the strain distribution around the screw, this prestress neglection has almost no influence on the global load-deformation behavior [18].

To reproduce a single-leg stance condition, a portion of the pubic symphysis and of the iliac crest were constrained [32] and the hip force representing a static single-leg stance task measured by Bergmann and colleagues [33]. The reaction force during single leg stance, obtained by Bergmann in ten patients wearing an instrumented hip implant, takes in consideration all the contractile structures that compose the upper thigh and the hip, beyond the presence of body weight. Here, the average value between the maximum and the minimum for each force component (resulting from a 100 kg patient) have been computed, obtaining a 2032 N resultant force (F_x = 651 N, F_y = −126.5 N, F_z = 1921 N). The resultant was applied according to a local reference system centered in the femoral head and with the x axis along to the medial—lateral direction, the y-axis along the antero-posterior direction and the z-axis along the cranio-caudal direction.

2.3. Interfragmentary Movement Analysis (IFM)

The stabilizing power of the plate-screws configurations were assessed according to the Perren's theory [34], which states that the presence of suitable axial and transversal strains at fracture gap could be advantageous for bone healing through the formation of

the bone callus. To compute the fracture gap strains, two local coordinate systems for the transverse fracture (in blue) and for the vertical component of T-shaped fracture (in red) were considered (Figure 5).

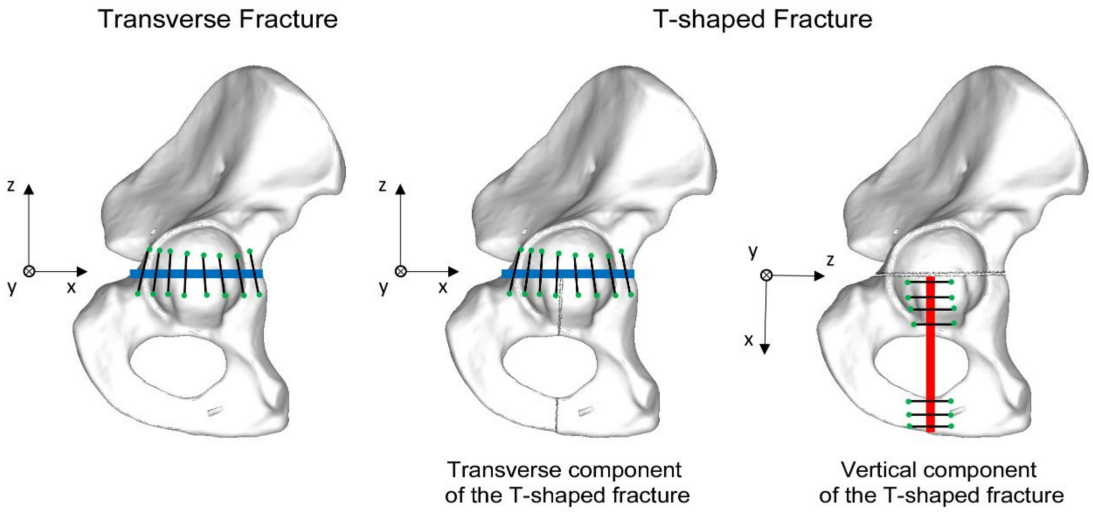

Figure 5. Reference systems and points couples selection in the transverse fracture (**left**) and in the T-shaped fracture (**right**). Note that the same blue reference system was applied for both the transverse fracture and the transverse component of the T-shaped fracture, while the red reference system was only applied for the vertical component of the T-shaped fracture. For both local reference systems, the z direction describes the compression and traction at the fracture region.

According to these local coordinate systems, the z-direction describes the compression and traction at the fracture region, conversely x- and y-directions represent movements that would bring misalignments of the bone stumps on the fracture plane.

To implement the gap analysis along the fractures brim, 22 equidistant couples of points crossing the fracture gap have been selected for the transverse fracture and 15 for the vertical component of T-shaped fracture; the same couples of points have been used for each model within the same fracture type (Figure 5). The incremental distances of each couple were measured and strains were then computed. The axial strain ε_{axial} has been obtained as the percentage variation in length along z direction over the respective mean fracture gap (GAP):

$$\varepsilon_{axial} = \varepsilon_z = \frac{\Delta z}{GAP} \cdot 100, \tag{1}$$

while for the shear strain, ε_{shear}, a strain magnitude was computed in order to obtain a unique value representing the fracture plane:

$$\varepsilon_{shear} = \sqrt{\varepsilon_x^2 + \varepsilon_y^2} = \sqrt{\left(\frac{\Delta x}{GAP} \cdot 100\right)^2 + \left(\frac{\Delta y}{GAP} \cdot 100\right)^2}, \tag{2}$$

where Δx, Δy and Δz are the maximum distance increment between each couple of points along the respective axis and according to the specific local reference system, and GAP is the mean fracture gap amplitude.

The so obtained strains have been classified in specific ranges (Table 5). For the axial strain, an optimal range, based on the limits defined by Perren's theory [34–36] and other studies [37–40], was selected. Conversely, the shear strain optimal range was defined based on the hypothesis that blocking sliding motions in the fracture plane would guarantee fracture extremities alignment during healing. An additional acceptable range was adopted for results visualization purposes to discriminate values that tends to optimal behaviors to those highly unacceptable for bone healing.

Table 5. Classification of axial and shear strain in the optimal, acceptable and unacceptable ranges.

Range	Axial Strain (%)	Shear Strain (%)
optimal	(−10, −2)	0
acceptable	(−15, −10)	(0, 15)
unacceptable	(−∞, −15)	(15, +∞)

3. Results

Results were at first analyzed focusing on Von Mises stresses and displacements distributions. In the regions of plate-bone contact, highest stresses are located at the pubic tubercle (Figure 6a). Only exception is the SQBP C1 plate in the T-shaped fracture, which shows a maximum stress of 174.4 MPa near screw hole number 15 (Figure 6b). For both fracture types fixed with the SQBP C2 plate, a clear reduction of the stresses at the pubic tubercle induced by the bone-plate larger contact is visible, whilst in proximity of the screw hole number 9, middle-low values of stresses (almost 20 MPa) can be noted (Figure 6b). Conversely, comparing the SQBP C1 and the SPP C2 fixation systems within the acetabular cup region (Figure 6c), in both fracture types the most solicited part consists in the antero-superior dial, condition determined by the direction of the external applied load, as already observed by Dalstra and Huiskes [41]. Here in fact, the maximal Von Mises stresses are on average 55 MPa with peaks up to 70 MPa; in the acetabulum remaining part the values range between 4 MPa (in the center of the acetabulum) and 23 MPa. From a qualitative evaluation, it was noted how the transverse fractures create more uniform stress distributions, suggesting a more homogeneous load transfer through the bone; this is probably due to the absence of the additional fracture of the T-shaped configuration, that represents an obstacle to the stress propagation.

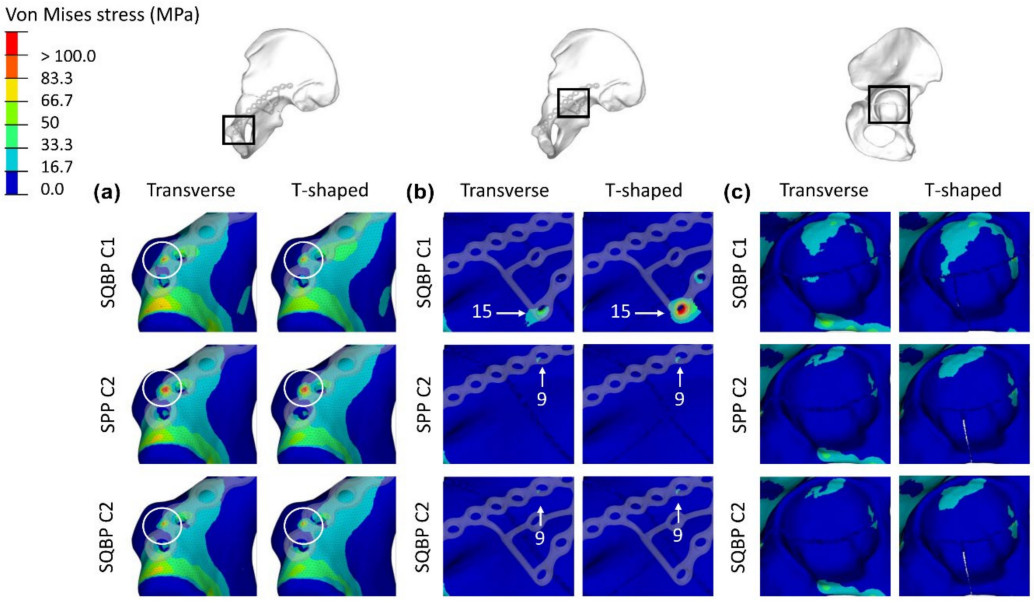

Figure 6. Von Mises stress distribution in the six analyzed configurations, with focus on the pubic tubercle region (**a**), the central screws region (**b**) and the acetabular region (**c**).

Comparing the SPP C2 and the SQBP C2 configurations, no macroscopic difference is visible in the stress distribution pattern within the same fracture type: stresses seem indeed to follow the same propagation curves.

Considering the hemipelvis globally, the highest value of stress among the combinations is found in the T-shaped fracture models: 382 MPa for the SQBP C1, 412 MPa for the SPP C2 and 337.8 MPa for the SQBP C2. This phenomenon is directly related to the conformation of the fracture which permits a rigid motion of the bone stumps decreeing

frictional contacts. In Table 6 the maximal Von Mises stresses found in the specific regions of the pelvis are reported.

Table 6. Maximum Von Mises stress (expressed in MPa) reached in the acetabular region, at the bone-plate contact and in the whole model.

Configuration	Fracture	Acetabulum	Bone-Plate Contact	Overall
SQBP C1	Transverse	62.4	102.1	102.1
	T-shaped	68.1	174.4	382.0
SPP C2	Transverse	30.9	161.6	161.6
	T-shaped	70.2	157.9	412.0
SQBP C2	Transverse	32.2	101.4	111.9
	T-shaped	70.5	99.1	337.8

The main outcome of the displacement analysis (Figure 7) is related to the differences between the two fracture types. In particular, all the T-shaped fracture models show the less stable behavior. In relation to the described situation, the SQBP C1 model has the highest magnitude of displacement equal to 3.1 mm, conversely in the SPP C2 model the maximum value is 2.33 mm. Observing the C2 models (both SPP and SQBP plates), similar behaviors arise. In fact, changing the plate, the differences are negligible: in both configurations the transverse fracture reports a maximal value of 0.96 mm.

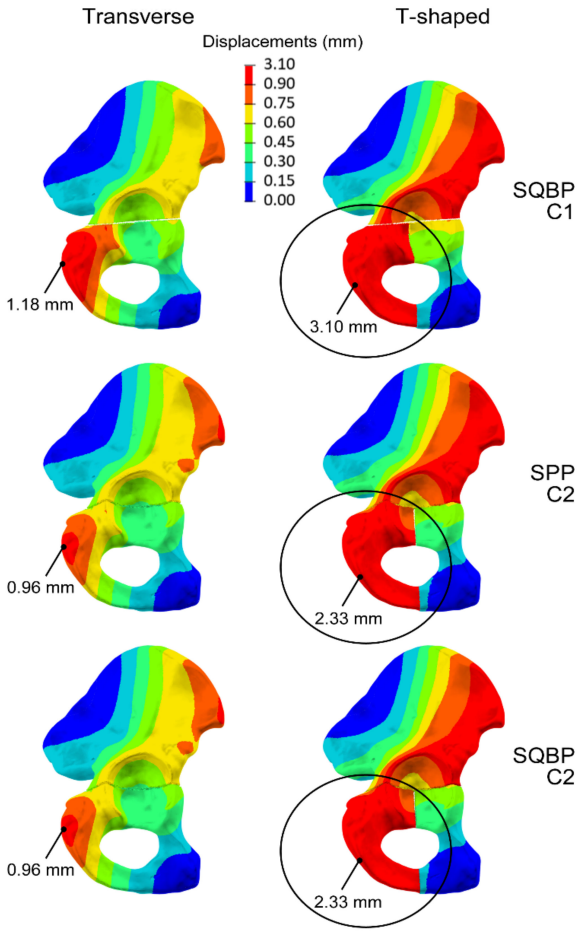

Figure 7. Displacement magnitude distribution in the six analyzed configurations: maximum value magnitude and location is shown for each model. Note that T-shaped fracture models show the less stable behavior, being the ischium region (black circles) the one subjected to major displacements.

3.1. Interfragmentary Movement Analysis (IFM)

3.1.1. Axial Strain

Comparing the configurations that differ both in terms of plate and screws configuration (SQBP C1 and SPP C2), it is possible to note two main differences regarding the elementary transverse fracture:

1. The median direction of the incremental distances (Figure 8b) of SPP C2 is mainly oriented towards a minimum axial expansion (median 1.57%) of the fracture gap; conversely SQBP C1 mainly brings the fracture gap towards minimum compressions (median −0.61%).
2. The slightly greater quantity in the SPP C2 model of observations satisfying the optimal range, ascertained by the percentage histogram in Figure 8a (36% against 31% of SQBP C1).

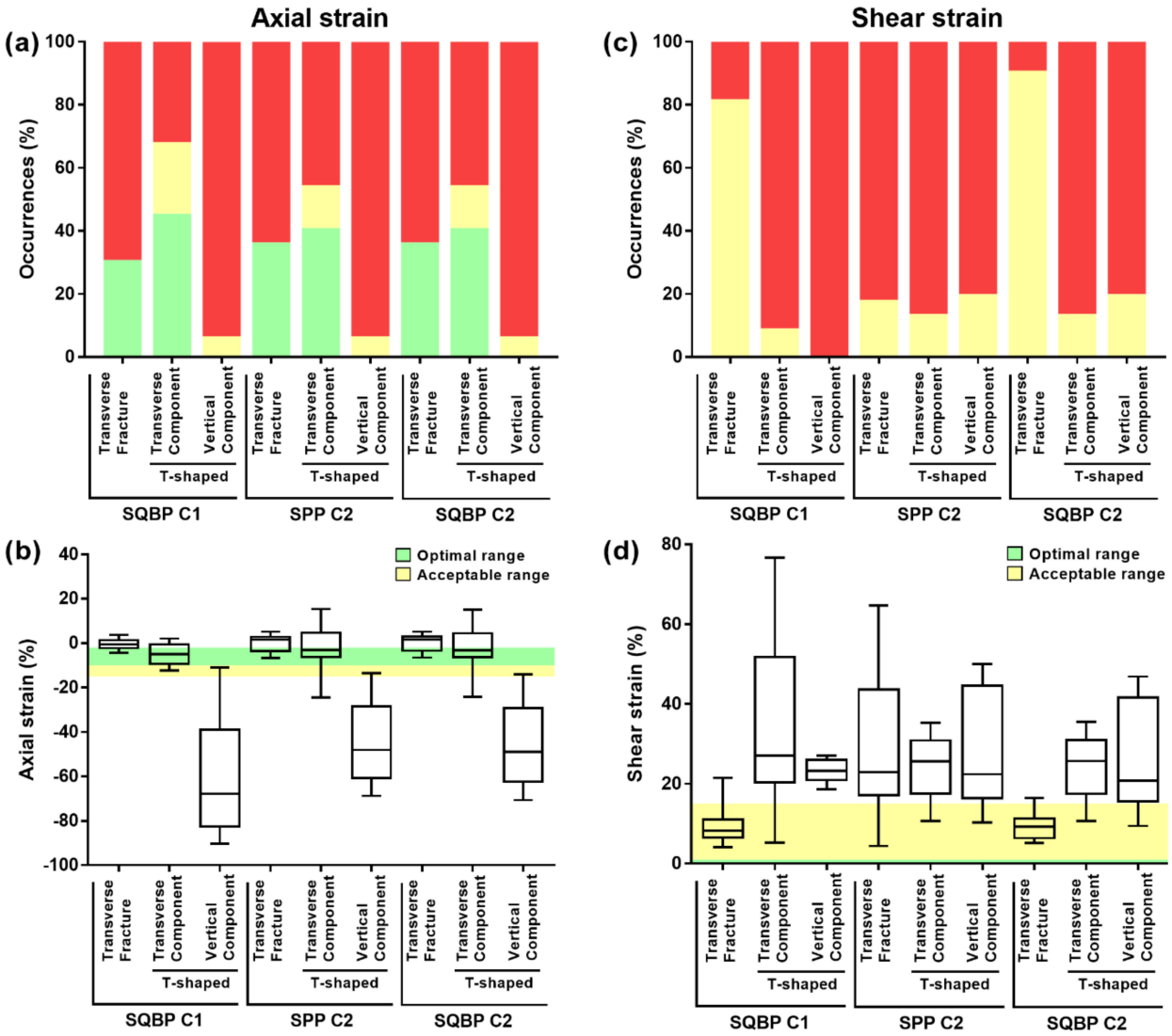

Figure 8. At the panel top, percentage histograms of axial (**a**) and shear (**c**) strains occurrences are shown. In detail, for each points couple the axial and the shear strains were computed according to equations 1 and 2. Obtained axial and shear strains for each points couple were classified according to the ranges listed in Table 5, and percentage occurrences were computed as the ratio between the number of points couples falling within the specific range and the total number of points couples. At the panel bottom, boxplots of axial (**b**) and shear (**d**) strain distributions are shown for each fracture. On each box, the central red mark indicates the distributions median, and the bottom and top edges of the blue box indicate the 25th and 75th percentiles, respectively. The whiskers represent the most extreme data points.

Comparing the T-shaped fracture, in its transverse component (Figure 8b) SQBP C1 shows a better performance, both related to the number of points couples belonging to the optimal range (45.5% vs. 41%) and to the acceptability range (68% vs. 55%). As far as the vertical component of the T shaped fracture is concerned, a very high axial compression is visible in both models, which generates an almost closure of the fracture gap. The minimal values are indeed respectively −90% (median −68%) for the SQBP C1 model and −69% (median −48%) for the SPP C2 model, which both result outside the optimal and the acceptable range (Figure 8b).

Comparing the C2 screw configuration models (SPP C2 and SQBP C2), the same behavior emerges according to the histogram percentages (Figure 8a): 36% of the couples belong to the optimal range for both the transverse elementary fractures, 41% of the occurrences satisfy the optimal range for both the transverse components of T-shaped fractures and, eventually, only almost 7% of occurrences are within the transition range as regards the two vertical components of T-shaped fractures.

3.1.2. Shear Strain

The distribution of shear strain among the various fractures shows that none of the configurations report an optimal behavior in blocking sliding motions in the fracture plane (0% shear strain). Comparing the models SQBP C1 and SPP C2, when the elementary transverse fracture is considered the former has lower shear strain values and almost 82% of the values are within the acceptable range (0–15)%, while the latter is characterized by a greater variability of shear strain in a range between 4% and 65% and with an acceptability percentage of 18% (Figure 8c). As far as the T-shaped fracture is concerned, in its transverse component a similar behavior between the two models is visible: for the SQBP C1 the shear strain values range between 5% and 77%, whilst for the SPP C2 range between 10% and 35%. Respectively, the percentage of couples of points within the acceptable range is 9% and 14%. For the vertical component of the T shaped fracture, the SQBP C1 values range between 18% and 27%, meaning that no points satisfy the acceptable range; in SPP C2 configuration, on the other hand, the shear strain is wider, between 10% and 50%, but with 20% of the points within the acceptable range.

If the C2 screws configurations models are compared, it can be noted that for the T-shaped fracture the differences are minimal: in the transverse fracture the range of shear strain distribution (10%, 36%) is almost identical (Figure 8d), and it is feasible to assess the same value of median equal to 26% with the same percentage of values belonging to the acceptable range (16.64%). In the vertical component of the T shaped fracture, a range of distribution equal to (10%, 50%) is reached, with median equal to 22%, for the SPP plate. The SQBP plate reaches a very similar range of values (9%, 47%) with median 21%. For both plates, the same percentage of 20% of the points within the acceptable range was computed. The substantial difference between the two plate is in the elementary transverse fracture: SPP plate has an acceptable percentage of 18% while the SQBP plate the percentage increases to 90%; in this latter, indeed, the range of shear strain is confined between 5 % and 16% with a median of 9%.

4. Discussion

The acetabular fractures treatment aims at the obtainment of an anatomical reduction, in order to minimize the risk of post-traumatic osteoarthritis, and of a stable fixation, able to maintain this reduction during the healing process. In transverse and T-shaped fractures, the entire medial portion of the acetabulum is detached from the upper portion so there are no bone structures capable of preventing medial subluxation of the femoral head. For this reason, traditionally, systems capable of fixing both columns are used in these fracture patterns. With this aim, plates that allow fixation of both columns and the quadrilateral plate through the anterior intrapelvic access have been developed. However, literature on the biomechanical stability guaranteed by these plates is limited.

The aim of this study was to compare, from a biomechanical point of view, the suprapectineal plate (SQBP) and the traditional reconstruction plate (SPP) in the treatment of transverse and T-shaped fractures of the acetabulum.

Observing the generated plate geometries, their property of following the articulate shapes of the hip stands out. The possibility to deform a 3D CAD plate design on the patient geometry, which immediately could fit on the patient's pelvic bone, would allow the surgeon to further minimize operation times and risks related to blood loss during surgical intervention with respect to the standard plane plates. Although rapid manufacturing techniques are emerging in the orthopedic devices production, the diffusion of these methodologies is still limited, especially in the field of load bearing plates [42]. Therefore, if the direct production of this patient specific plate through standard manufacturing technologies would comport realizability difficulties, an alternative approach could be implemented: thanks to the generation of a mold CAD model on the basis of the patient-adapted 3D CAD design, obtained in accordance with the procedure described in this work, the surgeon can model the plate on the physical mold manufactured in plastic materials through a low-cost 3D printing [43] thus obtaining a patient-adapted plate. This preoperative planning procedure, above all, would abolish any in-situ bending, reducing intervention time and preserving the patient from surgical risks as bleeding and infections [43].

Our plates comparison should be discussed in details. Focusing on the stress distribution, the models with the most solicited bone-plate contact zones are the ones with highest stress detected on the plate: the SPP plate showed the highest stresses manifestation. Furthermore, the SPP plate showed a more flexible behavior with respect to the SQBP plate because of its ability to adapt to the bone shape and thus it transfers more easily the load to the bone. The SQBP C2 configuration would result conversely stiffer and with lower strains present in the suprapectineal portion than the others, decreeing lower induced stresses to the bone. Even with equal screws configuration, the SQBP plate allows the reduction of stresses on the bone. Taking into account the results of the IFM, the infrapectineal portion of the SBQP plate, although without screws, brings improvements in the shear strain reduction (four times less than the standard plate: 65% vs. 16%). The same results have not been noticed on the axial compressions: on this axis, the two plates seem to similarly behave.

The SQBP plate with the screw configuration C1 achieves the best results in transverse fracture: it imposes an axial compression to the fracture gap (although the optimal range is only reached in 31% of points couples) and at the same time it minimizes the shear strain (which is within the acceptable range in 82% of the measurements).

The same behavior was not demonstrated in T shaped fractures: although the SQBP plate with the screw configuration C1 produces an optimal axial compression in 45.5% of the occurrences, shear strains are generated, reaching up the 77% of the average fracture gap wideness. The latter may compromise the secondary stability.

Regarding the axial strain in the vertical component of T-shaped fractures, all the plates and screw configurations are unable to prevent such a high compression of the fracture gap (the SPP C2 combination remains below 70% in compression whilst the SQBP C1 combination comports compression up to 90%).

From the shear strain point of view, the combination SQBP C1 has the most restrict distribution (reaching the value of 28%), probably due to the infrapectineal portion that would hold ischium stump with a better adhesion.

To the authors' knowledge, no computational study has involved the SQBP plate performance assessment, therefore, direct comparisons with literature are arduous. From a clinical point of view, our results support the findings by Kistler et al. [8], who biomechanically compared through cyclic mechanical testing five different fixation methods in transtectal transverse fractures. According to their results, authors stated that quadrilateral surface buttress plates are biomechanically comparable and, in some cases, superior to traditional forms of fixation in this synthetic hemipelvis model. Similar results have been

reported by Chen et al. [44], that evaluated the anterior column-posterior hemitransverse fractures. Chen and colleagues concluded that, although the suprapectineal pelvic brim plate with three periarticular long screws remains the gold standard in this fracture, the suprapectineal and infrapectineal QLS buttress plate are at least comparable with standard forms of fixation at resisting fracture motion and medial subluxation.

The results reported herein should be considered in the light of two major limitations, that could be addressed in future research. At first, fixed constraints at the pubic symphysis and at the iliac crest helped the authors to lighten the simulation, but represent a more critical situation than the physiological condition, characterized by flexible joints in these anatomical areas. Moreover, a single loading condition was investigated, neglecting muscle forces which could locally influence the stress state of the system. In any case, the comparative nature of the study makes the results obtained reliable, albeit not generalizable. Secondly, although according to literature two cartilages (one acetabular and one femoral) are present, a unique acetabular cartilage was here considered, attributing to its thickness the sum of the of the two original cartilages. This choice was considered reasonable given the purpose of the study. Lastly, the bonded contact imposed between bone and screws is a simplification of the real solicitation at the bone-screw interface, which could have influenced the distribution of stresses around the screws. However, fixations stability was assessed through the IFM analysis, which relies on the fracture fragments displacements. It is reported in the literature that, despite locally the bonded constraint does not allow relative motion between the screw and the bone, thus developing tension where separation would occur in reality, the interface modeling strategy has almost no influence on the global load-deformation behavior [18]. Therefore, the chosen approach did not influence, in the authors' opinion, the considerations made regarding the stability of the constructs.

5. Conclusions

This study, focused on the biomechanical comparison between the suprapectineal plate (SQBP) and the traditional reconstruction plate (SPP) in treatment of transverse and T-shaped fractures of the acetabulum, provided consistent outcomes in terms of internal fixation behaviors: the SQBP plate in transverse and T-shaped acetabular fractures results into lower bone stress, both in the screw tightening phase and in weight bearing, if compared to the SPP plate. Furthermore, the SQBP plate showed better performances in transverse fractures: in particular, the SQBP plate with 4 suprapectineal and 3 infrapectineal screws (C1 configuration) has the best performances for elementary transverse fracture. Moreover, the analysis shows comparable performances for the SPP plate and the SQBP plate with 6 suprapectineal screws in T-shaped fracture; the latter has the advantage of lesser bone stress. In conclusion, the suprapectineal plate seems to be a promising therapeutic option in transverse and T-shaped acetabular fractures, able to reduce bone stress values and to get results comparable, and in some cases superior, to traditional fixation.

Author Contributions: Conceptualization, A.A., S.A., A.M. and C.B.; methodology, A.D.P. and M.T.; software, A.D.P. and M.T.; validation, M.T.; formal analysis, A.D.P. and M.T.; investigation, A.D.P. and M.T.; resources, A.A. and C.B.; data curation, A.A.; writing—original draft preparation, A.D.P. and M.T.; writing—review and editing, all authors; visualization, A.D.P. and M.T.; supervision, C.B.; project administration, M.T., C.B., S.A., A.M. and A.A.; funding acquisition, C.B. and A.A. All authors have read and agreed to the published version of the manuscript.

Funding: This research received no external funding.

Institutional Review Board Statement: Not applicable.

Informed Consent Statement: Not applicable.

Data Availability Statement: The data presented in this study are available on request from the corresponding author.

Acknowledgments: We thank Daniele Russo e Daniele Guglielmino for their support.

Conflicts of Interest: The authors declare no conflict of interest.

References

1. Laird, A.; Keating, J.F. Acetabular fractures: A 16-year prospective epidemiological study. *J. Bone Jt. Surg. Br.* **2005**, *87*, 969–973. [CrossRef] [PubMed]
2. Rinne, P.P.; Laitinen, M.K.; Huttunen, T.; Kannus, P.; Mattila, V.M. The incidence and trauma mechanisms of acetabular fractures: A nationwide study in Finland between 1997 and 2014. *Injury* **2017**, *48*, 2157–2161. [CrossRef] [PubMed]
3. Judet, R.; Judet, J.; Letournel, E. Fractures of the acetabulum: Classification and surgical approach for open reduction. Preliminary report. *J. Bone Jt. Surg.-Am.* **1964**, *46*, 1615–1646. [CrossRef]
4. Tile, M.; Helfet, D.; Kellam, J.; Al, E. *Comprehensive Classification of Fractures in the Pelvis and Acetabulum*; Maurice E Müller Foundation: Berne, Switzerland, 1995.
5. Ma, K.; Luan, F.; Wang, X.; Ao, Y.; Liang, Y.; Fang, Y.; Tu, C.; Yang, T.; Min, J. Randomized, controlled trial of the modified Stoppa versus the ilioinguinal approach for acetabular fractures. *Orthopedics* **2013**, *36*, 1307–1315. [CrossRef]
6. Gras, F.; Marintschev, I.; Grossterlinden, L.; Rossmann, M.; Graul, I.; Hofmann, G.O.; Rueger, J.M.; Lehmann, W. The Anterior Intrapelvic Approach for Acetabular Fractures Using Approach-Specific Instruments and an Anatomical-Preshaped 3-Dimensional Suprapectineal Plate. *J. Orthop. Trauma* **2017**, *31*, e210–e216. [CrossRef]
7. Shazar, N.; Eshed, I.; Ackshota, N.; Hershkovich, O.; Khazanov, A.; Herman, A. Comparison of acetabular fracture reduction quality by the ilioinguinal or the anterior intrapelvic (modified Rives-Stoppa) surgical approaches. *J. Orthop. Trauma* **2014**, *28*, 313–319. [CrossRef]
8. Kistler, B.J.; Smithson, I.R.; Cooper, S.A.; Cox, J.L.; Nayak, A.N.; Santoni, B.G.; Sagi, H.C. Are quadrilateral surface buttress plates comparable to traditional forms of transverse acetabular fracture fixation? *Clin. Orthop. Relat. Res.* **2014**, *472*, 3353–3361. [CrossRef]
9. Zanetti, E.; Terzini, M.; Mossa, L.; Bignardi, C.; Costa, P.; Audenino, A.; Vezzoni, A. A structural numerical model for the optimization of double pelvic osteotomy in the early treatment of canine hip dysplasia. *Vet. Comp. Orthop. Traumatol.* **2017**, *30*, 256–264. [CrossRef]
10. Aldieri, A.; Terzini, M.; Osella, G.; Priola, A.M.; Angeli, A.; Veltri, A.; Audenino, A.L.; Bignardi, C. Osteoporotic Hip Fracture Prediction: Is T-Score-Based Criterion Enough? A Hip Structural Analysis-Based Model. *J. Biomech. Eng.* **2018**, *140*. [CrossRef]
11. Putzer, D.; Nogler, M.; Terzini, M.; Mannara, R.; Bignardi, C. A finite element analysis for a new short stem concept design with spherical bone interface for hip resurfacing. *Int. J. Mech. Eng. Technol.* **2018**, *9*, 923–935.
12. Terzini, M.; Zanetti, E.M.; Audenino, A.L.; Putame, G.; Gastaldi, L.; Pastorelli, S.; Panero, E.; Sard, A.; Bignardi, C. Multibody modelling of ligamentous and bony stabilizers in the human elbow. *Muscles. Ligaments Tendons J.* **2017**, *7*, 493. [CrossRef] [PubMed]
13. Putame, G.; Terzini, M.; Bignardi, C.; Beale, B.; Hulse, D.; Zanetti, E.; Audenino, A. Surgical Treatments for Canine Anterior Cruciate Ligament Rupture: Assessing Functional Recovery Through Multibody Comparative Analysis. *Front. Bioeng. Biotechnol.* **2019**, *7*, 180. [CrossRef] [PubMed]
14. Putame, G.; Pascoletti, G.; Terzini, M.; Zanetti, E.M.; Audenino, A.L. Mechanical Behavior of Elastic Self-Locking Nails for Intramedullary Fracture Fixation: A Numerical Analysis of Innovative Nail Designs. *Front. Bioeng. Biotechnol.* **2020**, *8*. [CrossRef] [PubMed]
15. Pascoletti, G.; Cianetti, F.; Putame, G.; Terzini, M.; Zanetti, E.M. Numerical simulation of an intramedullary Elastic Nail: Expansion phase and load-bearing behavior. *Front. Bioeng. Biotechnol.* **2018**, *6*. [CrossRef]
16. Mechlenburg, I.; Nyengaard, J.R.; Gelineck, J.; Soballe, K. Cartilage thickness in the hip joint measured by MRI and stereology—A methodological study. *Osteoarthr. Cartil.* **2007**, *15*, 366–371. [CrossRef]
17. Brandser, E.; Marsh, J.L. Review Acetabular Fractures: EasierClassification with a Systematic. *Am. J. Roentgenol.* **1998**, *171*, 1217–1228. [CrossRef]
18. MacLeod, A.R.; Pankaj, P.; Simpson, A.H.R.W. Does screw-bone interface modelling matter in finite element analyses? *J. Biomech.* **2012**, *45*, 1712–1716. [CrossRef]
19. Wieding, J.; Souffrant, R.; Fritsche, A.; Mittelmeier, W.; Bader, R. Finite element analysis of osteosynthesis screw fixation in the bone stock: An appropriate method for automatic screw modelling. *PLoS ONE* **2012**, *7*, e33776. [CrossRef]
20. Butz, K.D.; Chan, D.D.; Nauman, E.A.; Neu, C.P. Stress distributions and material properties determined in articular cartilage from MRI-based finite strains. *J. Biomech.* **2011**, *44*, 2667–2672. [CrossRef]
21. Chang, T.W.; Wu, C.H.; Liau, J.J.; Cheng, C.K. The Effect of Graft Strength on Knee Laxity and the In-Situ Forces of Grafts after Posterior Cruciate Ligament Reconstruction. In Proceedings of the World Congress on Medical Physics and Biomedical Engineering, Munich, Germany, 7–12 September 2009; Dössel, O., Schlegel, W.C., Eds.; Springer Berlin Heidelberg: Berlin/Heidelberg, Germany, 2010; pp. 809–812.
22. Tu, Y.K.; Chen, L.W.; Ciou, J.S.; Hsiao, C.K.; Chen, Y.C. Finite element simulations of bone temperature rise during bone drilling based on a bone analog. *J. Med. Biol. Eng.* **2013**, *33*, 269–274. [CrossRef]
23. ASM Aerospace Specification Metals Inc AISI Type 304 Stainless Steel. Available online: http://asm.matweb.com/search/SpecificMaterial.asp?bassnum=MQ304A (accessed on 1 December 2020).

24. Shockey, J.S.; von Fraunhofer, J.A.; Seligson, D. A measurement of the coefficient of static friction of human long bones. *Surf. Technol.* **1985**, *25*, 167–173. [CrossRef]
25. Damm, P.; Dymke, J.; Ackermann, R.; Bender, A.; Graichen, F.; Halder, A.; Beier, A.; Bergmann, G. Friction in total hip joint prosthesis measured in vivo during walking. *PLoS ONE* **2013**, *8*, e78373. [CrossRef] [PubMed]
26. Fuller, D.D. Theory and practice of lubrication for engineers (John Wiley & Sons, Chichester, 1984. £66.45 hardcover, 700 pp). *J. Synth. Lubr.* **1985**, *1*, 314. [CrossRef]
27. Hughes, A.N.; Jordan, B.A. The mechanical properties of surgical bone screws and some aspects of insertion practice. *Injury* **1972**, *4*, 25–38. [CrossRef]
28. Fitzpatrick, D.C.; Doornink, J.; Madey, S.M.; Bottlang, M. Relative stability of conventional and locked plating fixation in a model of the osteoporotic femoral diaphysis. *Clin. Biomech.* **2009**, *24*, 203–209. [CrossRef]
29. DePuy Synthes LCP Locking Compression Plate Surgical Technique. 2004. Available online: http://synthes.vo.llnwd.net/o16/LLNWMB8/INT%20Mobile/Synthes%20International/Product%20Support%20Material/legacy_Synthes_PDF/DSEM-TRM-0115-0278-3_LR.pdf (accessed on 1 December 2020).
30. Cordey, M.J.; Borgeaud, M.; Perren, S.M. Force transfer between the plate and the bone: Relative importance of the bending stiffness of the screws and the friction between plate and bone. *Int. J. Care Inj.* **2000**. [CrossRef]
31. Karnezis, I.A.; Miles, A.W.; Cunningham, J.L.; Learmonth, I.D. Axial preload in external fixator half-pins: A preliminary mechanical study of an experimental bone anchorage system. *Clin. Biomech.* **1999**, *14*, 69–73. [CrossRef]
32. Phillips, A.T.M.; Pankaj, P.; Howie, C.R.; Usmani, A.S.; Simpson, A.H.R.W. Finite element modelling of the pelvis: Inclusion of muscular and ligamentous boundary conditions. *Med. Eng. Phys.* **2007**, *29*, 739–748. [CrossRef]
33. Bergmann, G.; Bender, A.; Dymke, J.; Duda, G.; Damm, P. Standardized Loads Acting in Hip Implants. *PLoS ONE* **2016**, *11*, e0155612. [CrossRef]
34. Perren, S.M. Evolution of the internal fixation of long bone fractures. The scientific basis of biological internal fixation: Choosing a new balance between stability and biology. *J. Bone Jt. Surg. Br.* **2002**, *84*, 1093–1110. [CrossRef]
35. Caiti, G.; Dobbe, J.G.G.; Bervoets, E.; Beerens, M.; Strackee, S.D.; Strijkers, G.J.; Streekstra, G.J. Biomechanical considerations in the design of patient-specific fixation plates for the distal radius. *Med. Biol. Eng. Comput.* **2019**, *57*, 1099–1107. [CrossRef] [PubMed]
36. Kim, H.-J.; Kim, S.-H.; Chang, S.-H. Finite element analysis using interfragmentary strain theory for the fracture healing process to which composite bone plates are applied. *Compos. Struct.* **2011**, *93*, 2953–2962. [CrossRef]
37. Augat, P.; Burger, J.; Schorlemmer, S.; Henke, T.; Peraus, M.; Claes, L. Shear movement at the fracture site delays healing in a diaphyseal fracture model. *J. Orthop. Res.* **2003**, *21*, 1011–1017. [CrossRef]
38. Claes, L.E.; Meyers, N. The direction of tissue strain affects the neovascularization in the fracture-healing zone. *Med. Hypotheses* **2020**, *137*, 109537. [CrossRef] [PubMed]
39. Steiner, M.; Claes, L.; Ignatius, A.; Simon, U.; Wehner, T. Disadvantages of interfragmentary shear on fracture healing–mechanical insights through numerical simulation. *J. Orthop. Res. Off. Publ. Orthop. Res. Soc.* **2014**, *32*, 865–872. [CrossRef] [PubMed]
40. Epari, D.R.; Taylor, W.R.; Heller, M.O.; Duda, G.N. Mechanical conditions in the initial phase of bone healing. *Clin. Biomech.* **2006**, *21*, 646–655. [CrossRef]
41. Dalstra, M.; Huiskes, R. Load transfer across the pelvic bone. *J. Biomech.* **1995**, *28*, 715–724. [CrossRef]
42. Zanetti, E.M.; Aldieri, A.; Terzini, M.; Calì, M.; Franceschini, G.; Bignardi, C. Additively manufactured custom load-bearing implantable devices: Grounds for caution. *Australas. Med. J.* **2017**, *10*. [CrossRef]
43. Chana-Rodríguez, F.; Mañanes, R.P.; Rojo-Manaute, J.; Gil, P.; Martínez-Gómiz, J.M.; Vaquero-Martín, J. 3D surgical printing and pre contoured plates for acetabular fractures. *Injury* **2016**, *47*, 2507–2511. [CrossRef]
44. Chen, K.; Yang, F.; Yao, S.; Xiong, Z.; Sun, T.; Guo, X. Biomechanical Comparison of Different Fixation Techniques for Typical Acetabular Fractures in the Elderly: The Role of Special Quadrilateral Surface Buttress Plates. *J. Bone Jt. Surg. Am.* **2020**, *102*, e81. [CrossRef]